

Boundary Layer Analysis of MHD Newtonian/Non Newtonian Liquid Flow Due to Curved Stretching Surface with Irregular Heat Source/Sink and Frictional Heating Effects

G. P. Ashwinkumar

Department of Mathematics

Vijayanagara Sri Krishnadevaraya University, Ballari-583106, India.

Email: ashwinpuje@gmail.com

(Received November 15, 2020)

Abstract: Modeling and computational framework are carried out to explore the influence of irregular heat source/sink and viscous dissipation on magnetohydrodynamic flow of Newtonian/non-Newtonian liquid due to a curved stretching sheet. An appropriate similarity conversion is implemented to convert the basic flow equations into dimensionless ODE's and they being solved by means of Runge-Kutta method with shooting scheme. Numerical outcomes of drive, thermal and concentration distributions, also wall friction, thermal and mass transport rates are explored through graphical trends and tabular values. Simultaneous solutions are drawn for Newtonian and non-Newtonian liquids. The major findings of this study are rising the curvature parameter values inflates the momentum boundary layer, ergo develops the velocity distributions. Also, the heat transfer rate under the influence of irregular heat generation/absorption and dissipation effects is remarkably large for non-Newtonian liquid as compared with Newtonian liquid.

Keywords: MHD; Casson fluid; curved stretching surface; irregular heat source/sink; frictional heating; Slip effect

1. Introduction

Investigations entailing non-Newtonian liquid across a stretchable surface have been substantially increased owing to enormous practical applications viz. chemical, biological and pharmaceutical industries. In view of exceptional rheological properties of non-Newtonian liquids, they are massively utilized in engineering, technological and production

industries. And further honey, tooth paste, form oil etc. are few well known examples of these fluids. Keeping this in view, Vaidya et al.¹ deliberated the peristaltic flow of non-Newtonian liquid in a tapered artery. They revealed that, flow velocity is the regulating function of varying viscosity. Later, Waqas et al.² examined the impression of heat generation on the mixed convective flow of William fluid across an elongated surface with Fourier's and Fick's laws. It is seen influence of GFL over thermal distributions are more prominent than FL case. Influence of viscous dissipation on stagnation flow of Oldroyd-B liquid due to a Riga plate was numerically interpreted by Nayak et al.³. They confirmed the relaxation-retardation plays prominent role in escalating the thermal fields. Ibrahim and Zemedu⁴ used bvp4c MatLab code to inspect the impression of magnetic field on the flow of micropolar nanoliquid caused by a revolving disk. A similar kind of study with flow of micropolar liquid over a cylindrical pipe was carried out by Yadav and Verma⁵, they computed the simultaneous solutions for two distinct fluids. Moreover, investigations on the flow behavior of non-Newtonian liquids can be found in ref.⁶⁻¹⁰ by considering diverse aspects.

Boundary layer flow features caused by stretched surface of variable thickness has perceived abundant significance in the field of scientific, medical and industrial developments, Such applications includes paper production, drying of paper, hot rolling, textile machines, polymer processing etc. Abdelmalek et al.¹¹ studied the impression of Joule and frictional heating on nanoliquid flow along an elongated surface of non-uniform thickness. Later, Sindhu and Gireesha¹² examined the significance of nanoparticle shapes on hydrodynamic flow of magnetic nanoliquid across a microchannel with convective heating condition. They witnessed spherical shaped nanoparticles possess lowered thermal conductivity as equated with non-spherical case. Pandit and Sharma¹³ employed Wavelet scheme to resolve the equations of unsteady flow of nanoliquid passing through a rectangular passage. Similar kind of work carried by Ramesh et al.¹⁴ using hybridized nanoliquid flow across a cylinder. In recent period, several authors explored the investigations on analyzing heat transfer features of various fluids along diverse geometries¹⁵⁻¹⁸. Moreover, Amjad et al.¹⁹ deliberated the stagnation flow and thermal transfer attribute of micropolar nanoliquid across a curved elongated channel. They reflected the velocity and microrotation attributes are magnifying function of curvature criteria. Further, similar type of investigation was performed by Abbas et al.²⁰ and Kumar et al.²¹.

In the current technological and informative era researchers concentrating more on magnetohydrodynamic flow problems owing to the practical importance viz. power generators, droplet filters, plasma studies, drug treating, etc. Ramesh and Dewakar²² examined the impression of MHD on peristaltic flow of non-Newtonian liquid along an inclined channel. They perceived that angle of inclination has a tendency to augment the pressure difference and gradient. Later, the rheological response of CNT/Fe₃O₄ nanoliquid with magnetic field effect was experimentally studies by Talebizadehsardari et al.²³. They conveyed that impact of magnetic field over viscosity was negligible, when the applied strength was mere than 360mT. Moreover, plentiful number of authors²⁴⁻²⁷ performing investigations on this area.

Taking cues from above studies, we witness an ample number of studies available on Newtonian/non-Newtonian liquid flows across a curved elongated surface. Owing to this we examined the similarity solution of Newtonian/non-Newtonian fluid flows over a curved elongated surface with irregular heat generation/absorption and magnetic field effects. Various tests on numerical outcomes are performed to witness the significance of physical parameters utilized in modeled equations. Graphical and tabular outcomes are listed for drive, thermal and concentration attributes for several physical aspects.

2. Mathematical Formulation

We presumed the boundary layer nature of a Casson liquid caused by a curve shaped stretching surface of radius X . We suppose that (s, r) are the curvilinear coordinates and the fluid flow is time-independent for modeling the problem. Here s is the coordinate of the arc length in flow direction and r is normal to it, refer Fig.1. We presume that the sheet stretches in s -direction with velocity $u_o(s) = cs$, where c is a stretching constant. The B_0 is the magnitude of magnetic field applied in perpendicular to s coordinate as delineated in Fig.1. Here T_o, C_0 and T_∞, C_∞ are the temperature and concentration at the surface and ambient surface, respectively. The mathematical model of the problem is encompassed with irregular heat generation/absorption, frictional heating, chemical reaction magnetic field effects are taken into consideration.

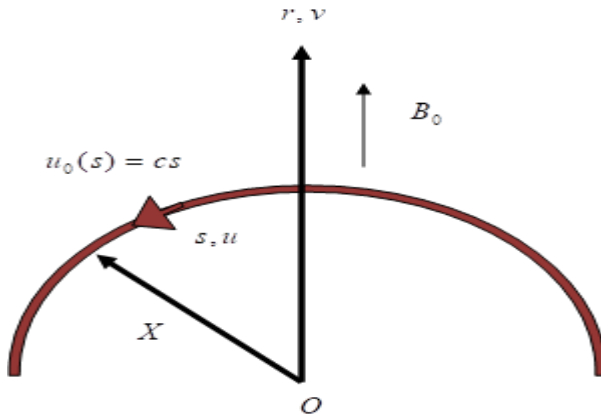


Figure 1. Flow geometry of the problem

Under these assumptions, the governing equations of Casson liquid flow with heat and mass transfer are provided as (Kumar et al.²¹),
Continuity equation

$$(2.1) \quad \frac{\partial}{\partial r}((X+r)v) + X \frac{\partial u}{\partial s} = 0,$$

Pressure distribution equation

$$(2.2) \quad \frac{1}{X+r} u^2 = \frac{1}{\rho} \frac{\partial p}{\partial r},$$

Momentum equation

$$(2.3) \quad \left(v \frac{\partial u}{\partial r} + \frac{X}{X+r} u \frac{\partial u}{\partial s} + \frac{1}{X+r} uv \right) = \frac{-X}{\rho(X+r)} \frac{\partial p}{\partial s} + \nu(1 + \beta^{-1})$$

$$\left(\frac{\partial^2 u}{\partial r^2} + \frac{1}{X+r} \frac{\partial u}{\partial r} - \frac{1}{(X+r)^2} u \right) - \frac{\sigma B_0^2 u}{\rho},$$

Energy equation

$$(2.4) \quad \rho c_p \left(\frac{X}{X+r} u \frac{\partial T}{\partial s} + v \frac{\partial T}{\partial r} \right) = k \left(\frac{1}{X+r} \frac{\partial T}{\partial r} + \frac{\partial^2 T}{\partial r^2} \right)$$

$$+\mu(1 + \beta^{-1})\left(\frac{\partial u}{\partial r} - \frac{u}{X+r}\right)^2 + Q_0(T - T_\infty) + q''' ,$$

Species diffusion equation

$$(2.5) \quad \left(\frac{X}{X+r}u \frac{\partial C}{\partial s} + v \frac{\partial C}{\partial r}\right) = D_B \left(\frac{1}{X+r} \frac{\partial C}{\partial r} + \frac{\partial^2 C}{\partial r^2}\right) - K(C - C_\infty),$$

The suitable boundary conditions of the problem are,

$$(2.6) \quad \begin{cases} u = u_0 = cs, v = 0, -k \frac{\partial T}{\partial r} = h_c(T_0 - T), -D_B \frac{\partial C}{\partial r} = h_d(C_0 - C), \text{ at } r = 0 \\ u \rightarrow 0; \frac{\partial u}{\partial r} \rightarrow 0, T \rightarrow T_\infty, C \rightarrow C_\infty \text{ as } r \rightarrow \infty, \end{cases}$$

Here u, v are the velocity components in r, s -directions, $\beta, \sigma, k, p, \nu, \mu, \rho, D_B, h_c, h_d, K, T, C$ are the Casson parameter, electrical conductivity, thermal conductivity, pressure, kinematic viscosity, dynamic viscosity, density, mass diffusivity, convective thermal and diffusion transport coefficients, first order chemical reaction parameter, fluid temperature and concentration, respectively.

The rheological equation Casson liquid is can be written as:

$$(2.7) \quad \tau_{ij} = \begin{cases} 2\left(\mu_B + \frac{p_y}{\sqrt{2\pi}}\right)e_{ij}, & \pi > \pi_c \\ 2\left(\mu_B + \frac{p_y}{\sqrt{2\pi_c}}\right)e_{ij}, & \pi < \pi_c \end{cases}$$

where $\pi = e_{ij}e_{ij}$ and e_{ij} represents the deformation rate in $(i, j)^{th}$ factor, π, π_c are the deformation rate and critical value, μ_B, p_z are the plastic dynamic viscosity and yield stress respectively.

In energy equation (2.4) $q''' = (ku_0 / sv)\{A^*(T_0 - T_\infty)f' + B^*(T - T_\infty)\}$, is the uneven heat source/sink parameter, in which A^* and B^* are the coefficients of space and temperature dependent heat source and sink respectively. If

positive values of A^* , B^* represents the heat generation and negative values of A^* and B^* depicts the heat absorption.

To transform the system of equations (2.1) to (2.5) into a dimensionless form, we introduced the following similarity transformations, which also satisfy the equation of continuity.

$$(2.8) \quad \begin{cases} u = csF'(\eta), v = \frac{-X}{X+r} \sqrt{cv} F(\eta), \eta = \sqrt{v^{-1}c} r, p = \rho c^2 s^2 P(\eta), \\ T = T_\infty + (T_0 - T_\infty)\theta(\eta), C = C_\infty + (C_0 - C_\infty)\phi(\eta). \end{cases}$$

In the above equations (2.8), the prime ' denotes the ordinary differentiation with respect to the similarity variable η . c is a positive constant, F' , Θ and Φ are the dimensionless velocity, temperature and concentration of the flow field respectively.

The equations corresponding to the pressure, momentum, energy and species diffusion equations (2.1), (2.2), (2.3), (2.4) and (2.5) are transformed with the aid of similarity transmutations (2.7), we obtain

$$(2.9) \quad (f')^2 = (\eta + \kappa)P',$$

$$(2.10) \quad \left(\frac{2\kappa}{\eta + \kappa} \right) P = (1 + \beta^{-1}) (f''' + (\eta + \kappa)^{-1} f'' - (\eta + \kappa)^{-2} f') \\ + \kappa(\eta + \kappa)^{-1} ff'' - \kappa(\eta + \kappa)^{-1} f'^2 + \kappa(\eta + \kappa)^{-2} ff' - Mf',$$

$$(2.11) \quad (\theta'' + (\eta + \kappa)^{-1} \theta') + (A^* f' + B^* \theta) + \text{Pr} (\kappa(\eta + \kappa)^{-1} f \theta' + Q\theta) \\ + EcM \text{Pr} f'^2 = 0,$$

$$(2.12) \quad \phi''(\eta + \kappa) + (1 + Sc\kappa f) \phi' - Cr Sc(\eta + \kappa) \phi = 0$$

By substituting the similarity transformations (2.8) in the boundary conditions (2.6) the transformed boundary conditions are given as,

$$(2.13) \quad \begin{cases} f = 0, f' = 1, \theta' = Bi_1(1 - \theta(0)), \phi' = Bi_2(1 - \phi(0)), & \text{at } \eta = 0, \\ f' \rightarrow 0, f'' \rightarrow 0, \theta \rightarrow 0, \phi \rightarrow 0, & \text{as } \eta \rightarrow \infty. \end{cases}$$

In the above transformed Eqs. (2.9)- (2.12), $\kappa = X\sqrt{\frac{c}{\nu}}$ is the Curvature parameter, $Ec = \frac{c^2 s^2}{c_p(T_0 - T_\infty)}$ is the Eckert number, $Pr = \frac{c_p \mu}{k}$ is the Prandtl number, $M = \frac{\sigma B_0^2}{\rho c}$ is the magnetic field parameter, $Sc = \frac{\nu}{D_B}$ is the Schmidt number, $Cr = \frac{K}{c}$ is the chemical reaction parameter, $Q = \frac{Q_0}{c(\rho c_p)}$ is the heat source/sink parameter, $Bi_1 = \frac{h_c B_0^2}{k} \sqrt{\frac{\nu}{c}}$, $Bi_2 = \frac{D_B}{h_d} \sqrt{\frac{\nu}{c}}$ is are the thermal and mass transport Biot numbers respectively. on eradicating the pressure P from the Eqs. (2.9) and (2.10), we get

$$(2.14) \quad \begin{aligned} & (1 + \beta^{-1})((\eta + \kappa)^3 f^{iv} + 2f'''(\eta + \kappa)^2 - (\eta + \kappa)f'' + f') \\ & - \kappa(\eta + \kappa)^{-1}(ff'' - ff''') - \kappa(\eta + \kappa)^{-2}(f'^2 - ff''') \\ & - \kappa(\eta + \kappa)^{-2}f'' - M(f'' + f'(\eta + \kappa)^{-1}) = 0. \end{aligned}$$

The quantities of practical interest engineering are Skin-friction coefficient C_f , Nusselt and numbers Nu_s, Sh_s respectively given by

$$(2.15) \quad C_f \sqrt{Re_s} = (1 + \beta^{-1})(\kappa f''(0) - f'(0)),$$

$$(2.16) \quad Nu_s (Re_s)^{-1/2} = -\theta'(0),$$

$$(2.17) \quad Sh_s (Re_s)^{-1/2} = -\phi'(0),$$

where $Re_s = \frac{u_w s}{\nu}$ is the local Reynolds number.

3. Results and Discussions

The transformed equations (2.11)-(2.12) and (2.14) are highly nonlinear and coupled in nature. These equations along with boundary restrictions in

eq. (2.13) are solved using $R-K$ based shooting scheme. Further, the impression of numerous physical aspects viz. magnetic field M , curvature parameter κ , Prandtl number Pr , thermal and solutal Biot numbers Bi_1 , Bi_2 Schmidt number Sc , chemical reaction Cr , viscous dissipation Ec , space and time dependent heat source/sink A^* , B^* thermal radiation R and Casson parameter β over the flow determining profiles are depicted via plots i.e. (2) to (30). For numerical calculation, we allotted the parametric values as

$$M = 0.9; \kappa = 5; Ec = 1.2; A^* = 0.1; B^* = 0.1; \beta = 1;$$

$$R = 0.2; Bi_1 = 0.3; Bi_2 = 0.3; Pr = 6.2; Sc = 1.5; Cr = 0.1;$$

in the entire study, unless they are specified in respective plots. Here $f''(\eta)$, $\theta(\eta)$, C_f , Nu_x , Sh_x depicts the velocity curves, temperature curves, skin friction coefficient, local Nusselt and Sherwood number, respectively. We also witnessed the flow nature of two different solutions namely non-Newtonian fluid and Newtonian liquid they are displayed as solid line and dashed line, respectively.

Figs. 2–3 depicted to witness the essence of M over $f''(\eta)$ and $\theta(\eta)$ for both the solutions. We see that growing applied magnetic field, downturn the flow of fluid and upturn the thermal field. This happens because of development of flow resistive type of force named as Lorentz force. It is also evident that, impact of M over non-Newtonian fluid is significantly high as equated with Newtonian fluid. The significance of κ on $f''(\eta)$, $\theta(\eta)$ and $\phi(\eta)$, is unveiled in Figs. 4-6. It is manifest that ascending values of κ levitate $f''(\eta)$ and diminishes $\theta(\eta)$ and $\phi(\eta)$. Generally, improved values of κ leads to enlarge the radius of the curved surface. Consequently, fluid motion nimble over the surface. Hence the aforementioned results of the three profiles are perceived. It also interesting to notice that, influence of κ is remarkably high in non-Newtonian fluid than Newtonian fluid. Figs.7-11 explore the significance of Ec, R, A^*, B^* and Pr over the thermal profiles, respectively. It infers that thermal fields are increasing functions of Ec, R, A^*, B^* and Pr . Physically, Eckert number is the ratio of kinetic energy to the enthalpy difference. While magnified values of Ec amplifies the kinetic energy. Ergo, develops the temperature of the fluid. Rising R, A^* and B^* values supplies addition thermal energy to the flow of fluid owing to the radiative heat flux. Further, larger the Pr values

declines the thermal fields near the boundary, this is due to reduction in thermal diffusivity with increase in Pr values.

Figs. 12-13 reveal the reverberation of Bi_1 and Bi_2 on the thermal and concentration fields, respectively. It clears that, escalating values of Bi_1 enhances the thermal profiles. Generally, rise in Bi_1 boosts the heat transfer process through convection due to this we notices the augmentation in temperature fields. Further, ascending values of Bi_2 diminishes the mass diffusivity. Consequently the concentration profile declines. Figs. 14-15 portray the changes in $\phi(\eta)$ for dissimilar values of Sc and Cr . It is conspicuous that, growth in the values of Sc boosts the concentration fields, but it shows reverse trend for Cr . Customarily, an increment in Cr declines the solutal boundary layer thickness and enhances mass transfer. Impression of Casson parameter on $f''(\eta)$, $\theta(\eta)$ and $\phi(\eta)$ is illustrated in Figs.16-18. It is witnessed; all the three profiles are decreasing function of dissimilar values of β . Physically, escalating values of β declines the momentum thermal boundary layer thickness. Ergo, declines the velocity and thermal profiles.

Figs 19-26 deployed to witness the impression of $M, Ec, A^*, B^*, Pr, Bi_1, \kappa$ and β on rate of thermal transport, respectively. It is evident, the thermal transport rate is increasing function of M, Ec, A^*, B^*, Pr and Bi_1 , but a reverse trend is observed for κ and β . And also, the thermal transport rate in non-Newtonian liquid is remarkably large as equated with Newtonian liquid. The influence of M, κ , and Sc, Cr on Skin friction coefficient and local Sherwood number is deployed Figs. 27-28 and 29-30 respectively. It is clear that C_f, Sh_x are decelerating functions of M, κ , and Sc, Cr . Table 1 portrays the validation of the present outcomes with the existing outcomes and a excellent concurrence is found among the results for limiting case.

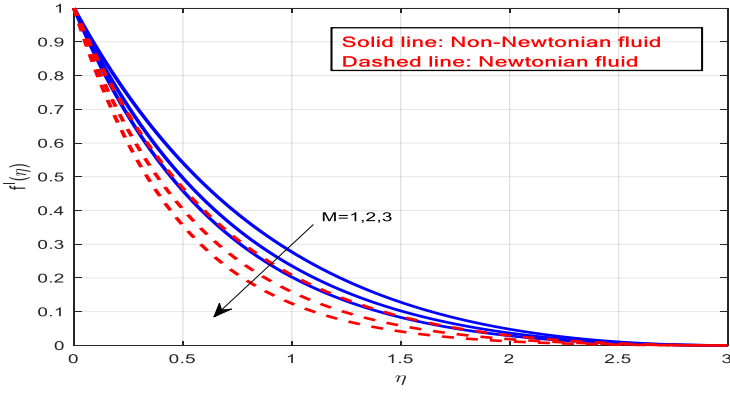


Figure 2. Impression of M on $f'(\eta)$

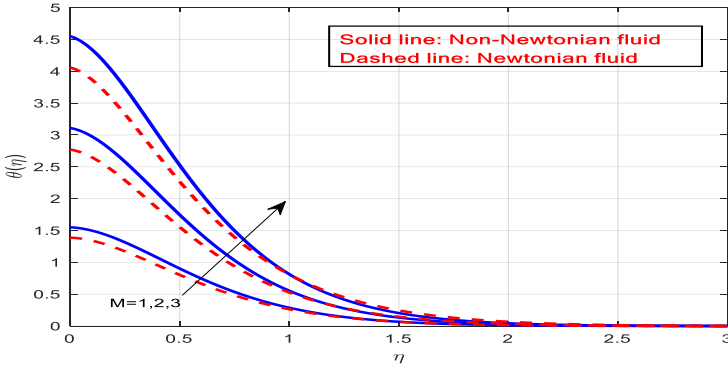


Figure 3. Impression of M on $\theta(\eta)$

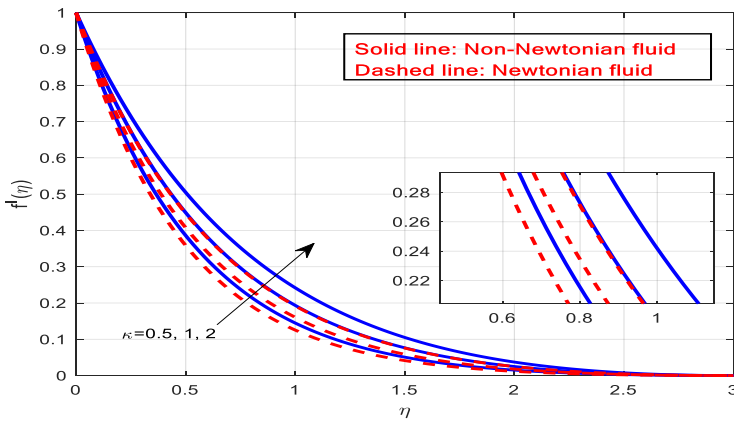


Figure 4. Impression of κ on $f'(\eta)$

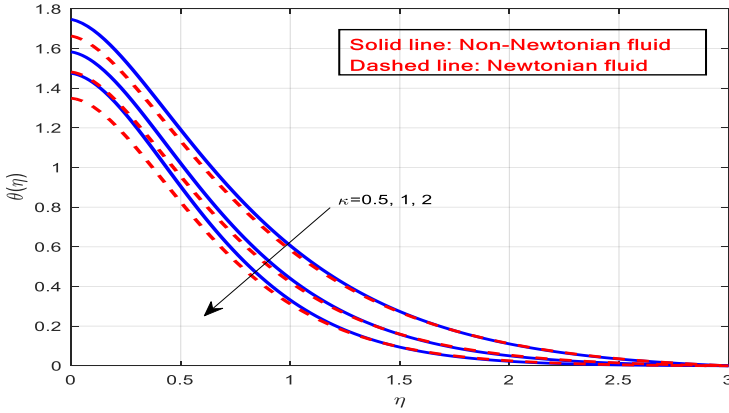


Figure 5. Impression of κ on $\theta(\eta)$

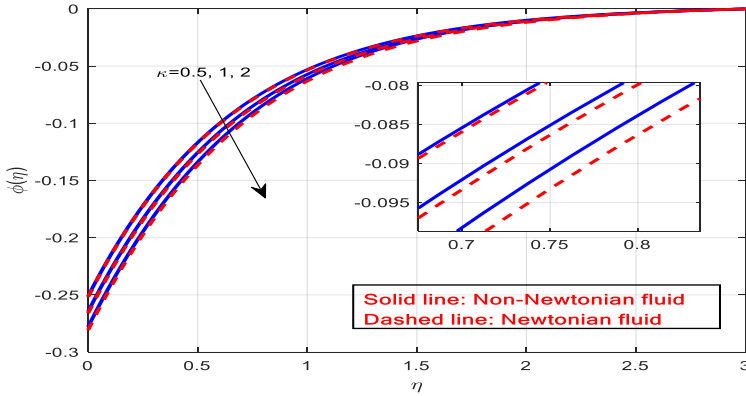


Figure 6. Impression of κ on $\phi(\eta)$

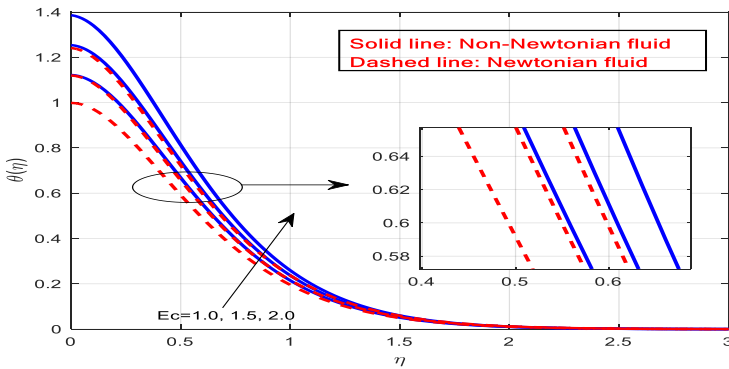


Figure 7. Impression of Ec on $\theta(\eta)$

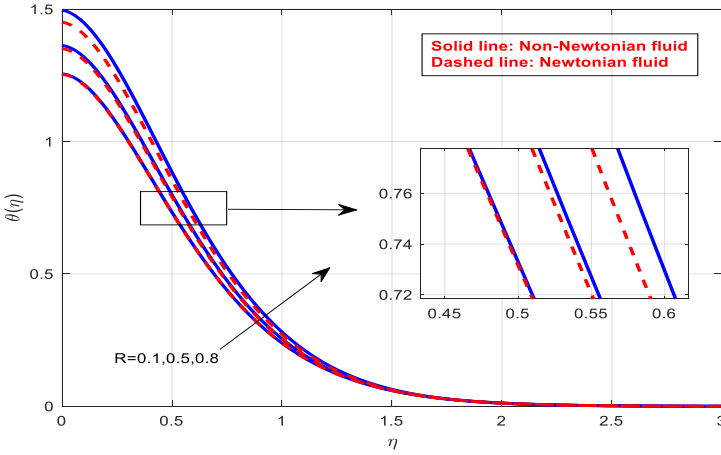


Figure 8. Impression of R on $\theta(\eta)$

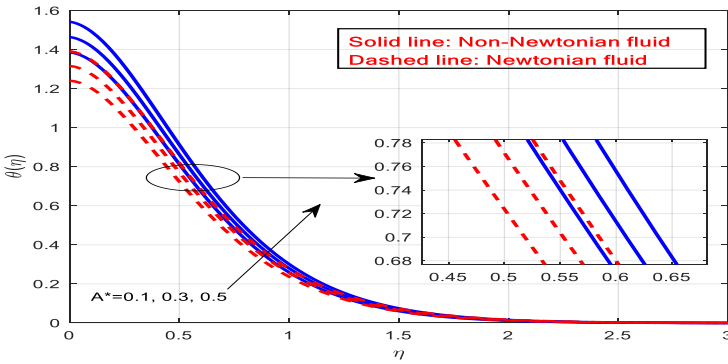


Figure 9. Impression of A^* on $\theta(\eta)$

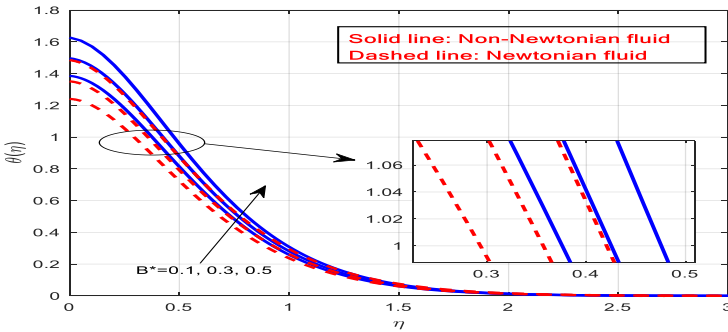


Figure 10. Impression of B^* on $\theta(\eta)$

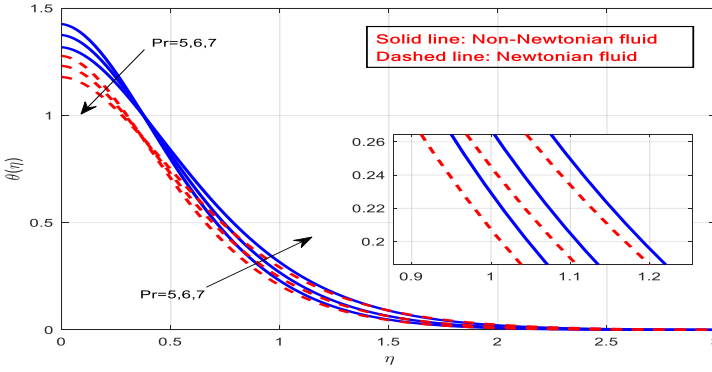


Figure 11. Impression of Pr on $\theta(\eta)$

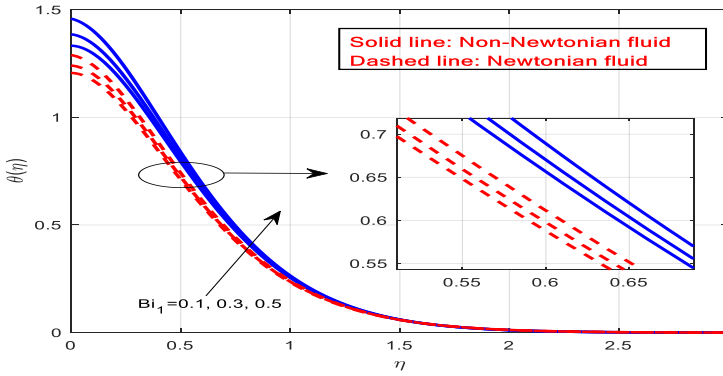


Figure 12. Impression of Bi_1 on $\theta(\eta)$

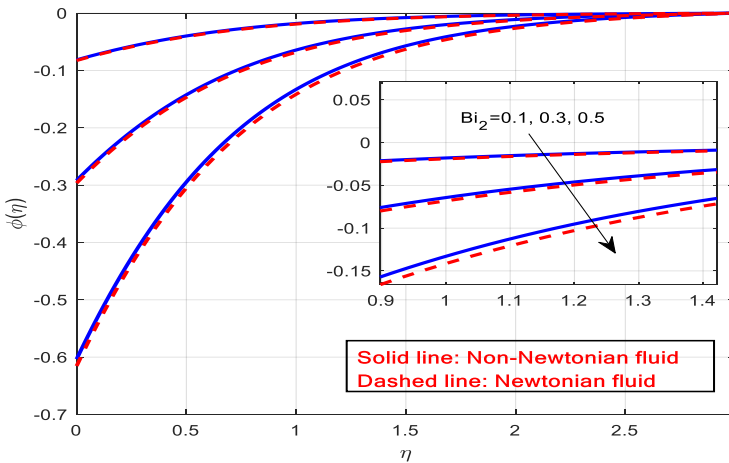


Figure 13. Impression of Bi_2 on $\phi(\eta)$

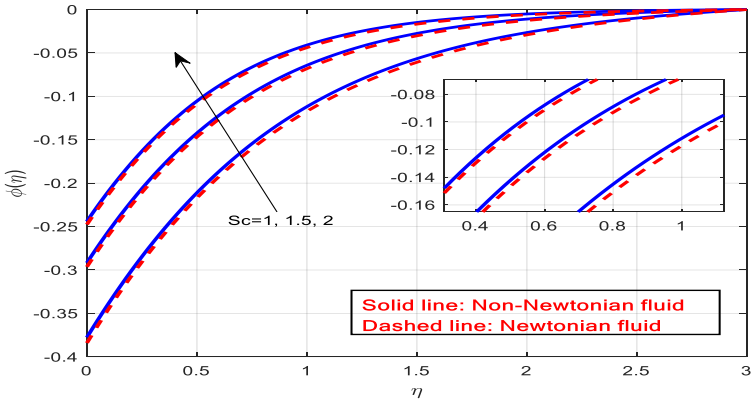


Figure 14. Impression of Sc on $\phi(\eta)$

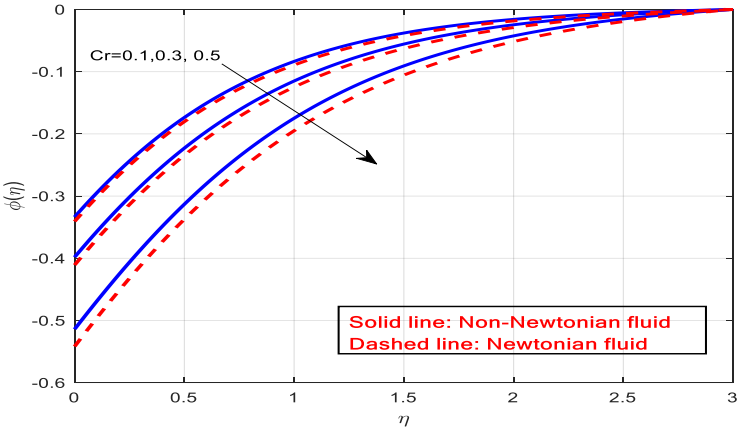


Figure 15. Impression of Cr on $\phi(\eta)$

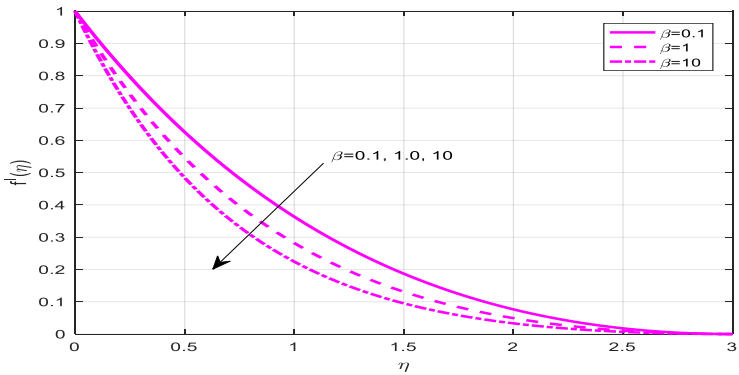


Figure 16. Impression of β on $f'(\eta)$

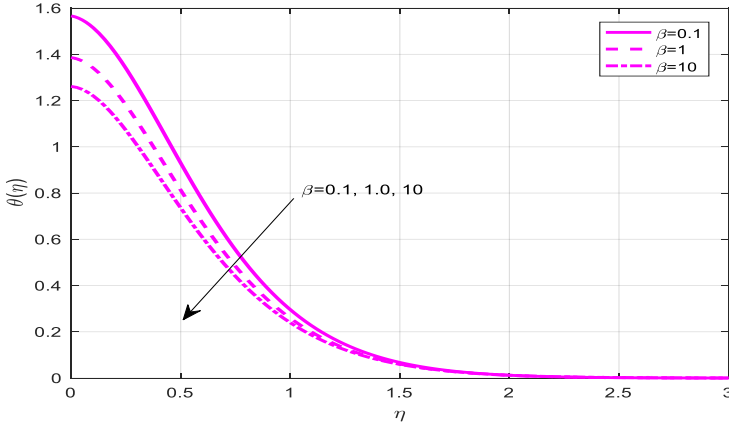


Figure 17. Impression of β on $\theta(\eta)$

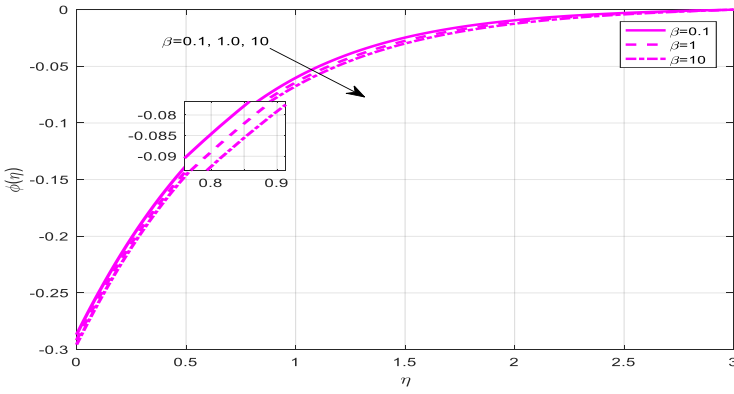


Figure 18. Impression of β on $\phi(\eta)$

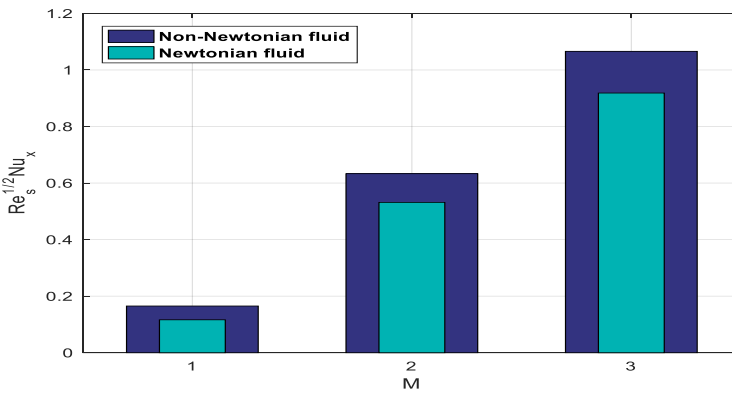


Figure 19. Impression of M on Nusselt number

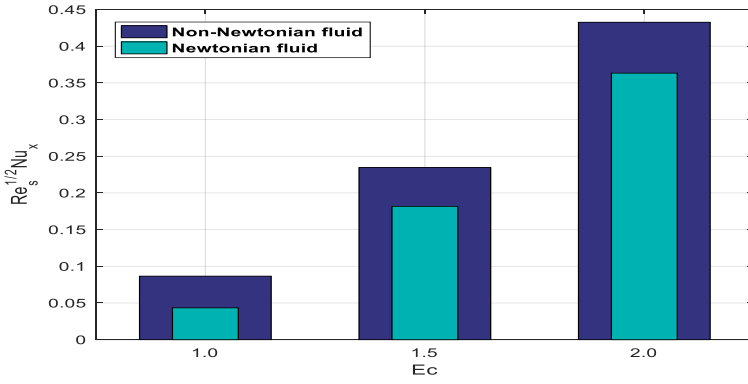


Figure 20. Impression of Ec on Nusselt number

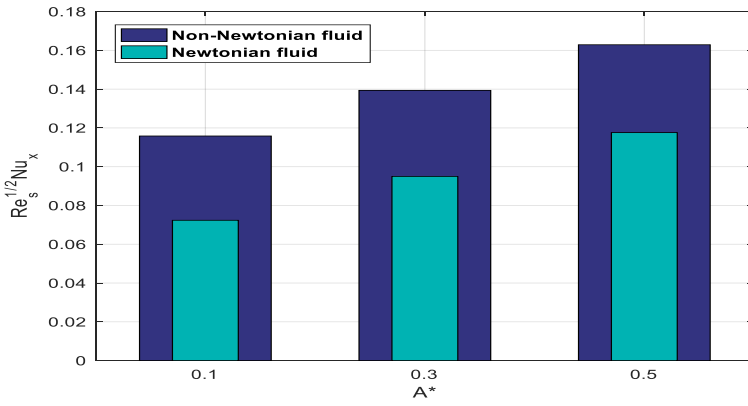


Figure 21. Impression of A^* on Nusselt number

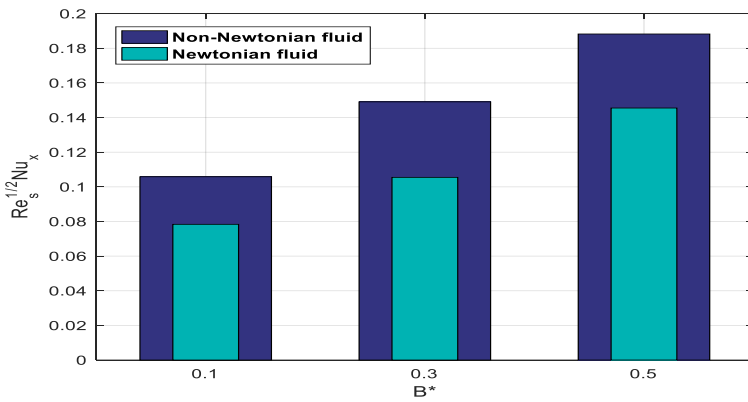


Figure 22. Impression of B^* on Nusselt number

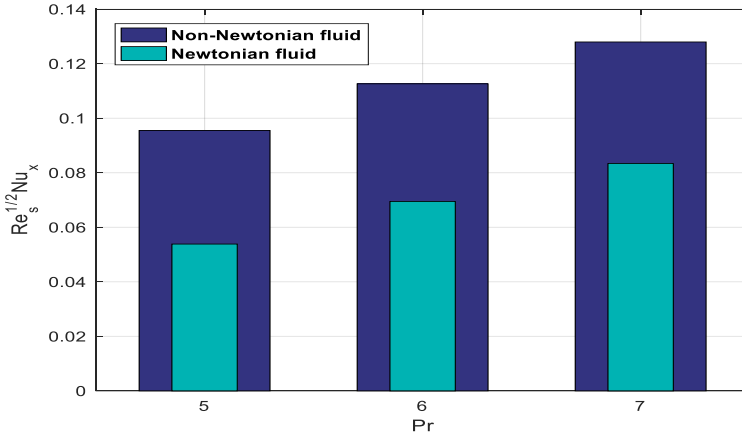


Figure 23. Impression of Pr on Nusselt number

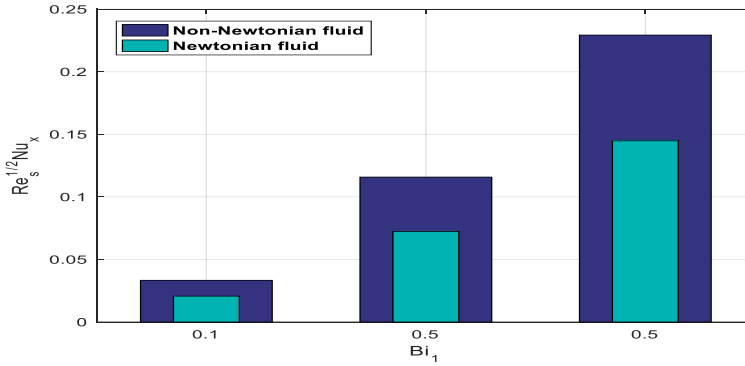


Figure 24. Impression of Bi_1 on Nusselt number

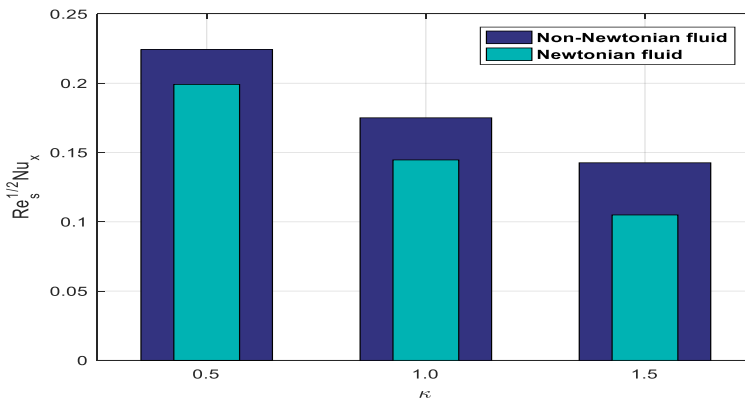


Figure 25. Impression of κ on Nusselt number

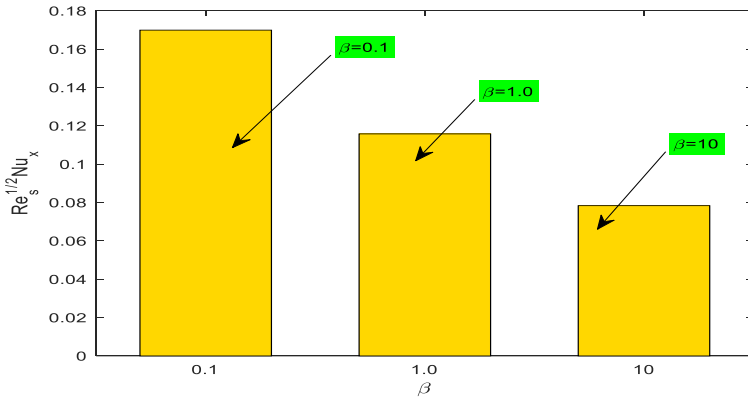


Figure 26. Impression of β on Nusselt number

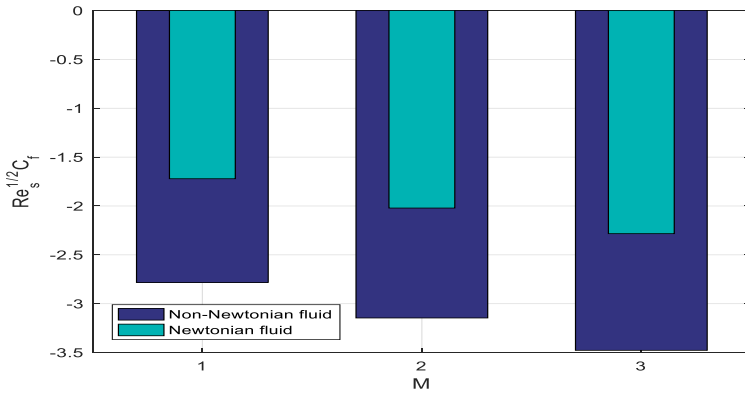


Figure 27. Impression of M on Skin friction factor

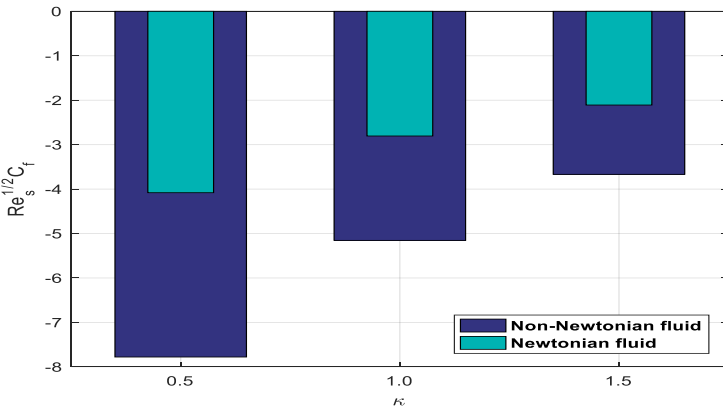


Figure 28. Impression of κ on Skin friction factor

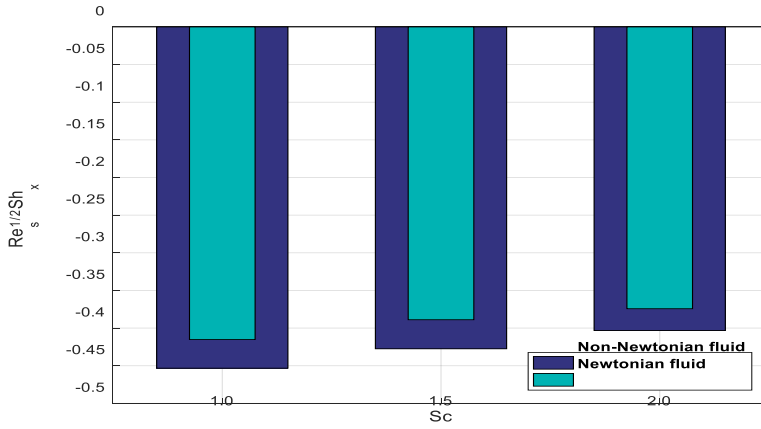


Figure 29. Impression of Sc on Sherwood number

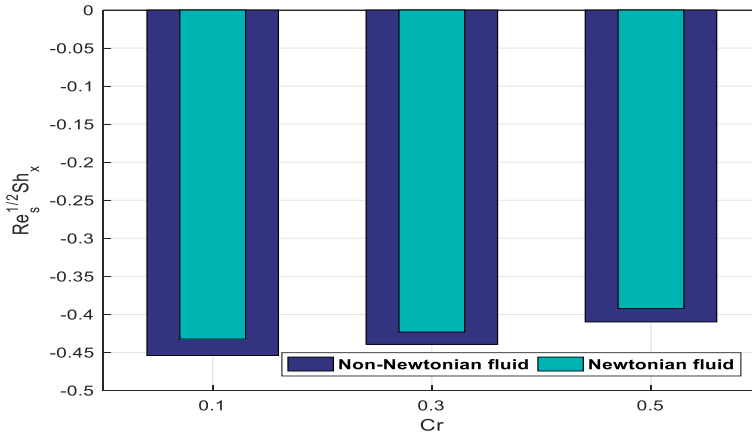


Figure 30. Impression of Cr on Sherwood number

Table 1 Validation of the outcomes of $f''(0)$ for various κ when $\beta \rightarrow \infty$

κ	Kumar et al. ²¹	Present results
0.1	-4.0251	-4.025253
1.0	-2.3950	-2.395124
10	-2.0086	-2.008757

4. Conclusions

The present investigation delivers the significance of frictional heating and uneven heat generation/absorption effect on the MHD flow of Newtonian/non-Newtonian fluid about a curved stretching surface. Simultaneous solutions are deployed for Newtonian and non-Newtonian fluid cases using plots. Few significant facts are outlined below.

- (a) Magnifying values of M , Ec , R , A^* , B^* and Pr upshots the temperature fields but a reverse nature is witnessed for κ .
- (b) Curvature parameter has a proclivity to inflate the momentum boundary layer. Ergo, develops the velocity fields.
- (c) Impact of physical parameters on non-Newtonian fluid is significantly large as matched with Newtonian fluid.
- (d) The parameters M , κ and Sc , Cr have propensity to lessen the skin friction factor.
- (e) Rate of thermal transport under the influence of M , Ec , A^* , B^* , Pr , Bi_1 is notably large for non-Newtonian fluid as equated with Newtonian fluids.

References

1. H. Vaidya, C. Rajashekhar, B. B. Divya, G. Manjunatha, K. V. Prasad and I. L. Animasaun, Influence of Transport Properties on the Peristaltic MHD Jeffrey Fluid Flow Through a Porous Asymmetric Tapered Channel, *Results Phys.*, **18** (2020), 103295, doi:10.1016/j.rinp.2020.103295.
2. M. Waqas, M. I. Khan, Z. Asghar, S. Kadry, Y. M. Chu and W. A. Khan, Interaction of Heat Generation in Nonlinear Mixed/Forced Convective Flow of Williamson Fluid Flow Subject to Generalized Fourier's and Fick's Concept, *J. Mater. Res. Technol.*, **9** (2020) 11080–11086, doi:10.1016/j.jmrt.2020.07.068.
3. M. K. Nayak, S. Saranya, B. Ganga, A. K. A. Hakeem, R. P. Sharma and O. D. Makinde, Influence of Relaxation-Retardation Viscous Dissipation on Chemically Reactive Flow of Oldroyd-B Nanofluid With Hyperbolic Boundary Conditions, *Heat Transf.*, (2020), 1-23, doi:10.1002/htj.21861.
4. W. Ibrahim, C. Zemedu, MHD Nonlinear Natural Convection Flow of a Micropolar Nanofluid Past a Nonisothermal Rotating Disk, *Heat Transf.*, (2020), 1-32, doi:10.1002/htj.21894.
5. P. K. Yadav and A. K. Verma, Analysis of Immiscible Newtonian and Non-Newtonian Micropolar Fluid Flow Through Porous Cylindrical Pipe Enclosing a Cavity, *Eur. Phys. J. Plus*, **135** (2020), 1-35, doi:10.1140/epjp/s13360-020-00672-6.
6. H. Ullah, M. I. Khan and T. Hayat, Modeling and Analysis of Magneto-Carreau Fluid with Radiative Heat Flux: Dual Solutions About Critical Point, *Adv. Mech. Eng.*, **12** (2020), 1-10, doi:10.1177/1687814020945477.

7. C. Sulochana, G. P. Ashwinkumar and N. Sandeep, Effect of Frictional Heating on Mixed Convection Flow of Chemically Reacting Radiative Casson Nanofluid Over an Inclined Porous Plate, *Alexandria Eng. J.*, **57** (2018), 2573-2584.
8. R. Mahato and M. Das, Effect of Suction/Blowing on Heat-Absorbing Unsteady Radiative Casson Fluid Past a Semi-Infinite Flat Plate with Conjugate Heating and Inclined Magnetic Field, *Pramana -J. Phys.*, **94** (2020), 1–16, doi:10.1007/s12043-020-01990-1.
9. G. P. Ashwinkumar and C. Sulochana, Effect of Radiation Absorption and Buoyancy Force on the MHD Mixed Convection Flow of Casson Nanofluid Embedded with Al50Cu50 Alloy Nanoparticles, *Multidiscip. Model. Mater. Struct.*, **14** (2018), 1082-1100.
10. M. Hassan, A. Issakhov, M. El Haj Assad, E. H. Bani Hani, M. Rahimi-Gorji, S. Nadeem and S. U. D. Khan, The Effects of Zero and High Shear Rates Viscosities on the Transportation of Heat and Mass in Boundary Layer Regions: A Non-Newtonian Fluid with Carreau Model, *J. Mol. Liq.*, **317** (2020) 113991, doi:10.1016/j.molliq-2020.113991.
11. Z. Abdelmalek, I. Khan, M. W. A. Khan, K. U. Rehman and E. S. M. Sherif, Computational Analysis of Nano-Fluid Due to a Non-Linear Variable Thickened Stretching Sheet Subjected to Joule Heating and Thermal Radiation, *J. Mater. Res. Technol.*, **9** (2020), 11035-11044, doi:10.1016/j.jmrt.2020.07.085.
12. S. Sindhu and B. J. Gireesha, Effect of Nanoparticle Shapes on Irreversibility Analysis of Nanofluid in a Microchannel with Individual Effects of Radiative Heat Flux, Velocity Slip and Convective Heating, *Heat Transf.*, (2020), 1-17. doi:10.1002/htj-21909.
13. S. Pandit and S. Sharma, Wavelet Strategy for Flow and Heat Transfer in CNT-Water Based Fluid with Asymmetric Variable Rectangular Porous Channel, *Eng. Comput.*, (2020), doi:10.1007/s00366-020-01139-z.
14. G. K. Ramesh, S. Manjunatha, G. S. Roopa and A. J. Chamkha, Hybrid (ND-Co3O4/EG) Nanofluid Through a Permeable Cylinder Under Homogeneous-Heterogeneous Reactions and Slip Effects, *J. Therm. Anal. Calorim.*, (2020), doi:10.1007/s10973-020-10106-1.
15. E. G. Ushachew, M. K. Sharma and O. D. Makinde, Heat Convection in Micropolar Nanofluid Through Porous Medium-Filled Rectangular Open Enclosure: Effect of an Embedded Heated Object with Different Geometries, *J. Therm. Anal. Calorim.*, (2020), doi:10.1007/s10973-020-10118-x.
16. Usman, P. Lin and A. Ghaffari, Steady Flow and Heat Transfer of the Power-Law Fluid Between Two Stretchable Rotating Disks with Non-Uniform Heat Source/Sink, *J. Therm. Anal. Calorim.*, (2020), doi:10.1007/s10973-020-10142-x.
17. F. Mebarek Oudina, R. Bessaih, B. Mahanthesh, A. J. Chamkha and J. Raza, Magneto-Thermal-Convection Stability in an Inclined Cylindrical Annulus Filled with a Molten Metal, *Int. J. Numer. Methods Heat Fluid Flow*, (2020), doi:10.1108/HFF-05-2020-0321.

18. F. Hussain, A. Hussain and S. Nadeem, Thermophoresis and Brownian Model of Pseudo-Plastic Nanofluid Flow over a Vertical Slender Cylinder, *Math. Probl. Eng.*, **2020** (2020), 1-10, doi:10.1155/2020/8428762.
19. M. Amjad, I. Zehra, S. Nadeem and N. Abbas, Thermal Analysis of Casson Micropolar Nanofluid Flow Over a Permeable Curved Stretching Surface Under the Stagnation Region, *J. Therm. Anal. Calorim.*, (2020), doi:10.1007/s10973-020-10127-w.
20. Z. Abbas, M. Naveed and M. Sajid, Heat Transfer Analysis for Stretching Flow Over A Curved Surface With Magnetic Field, *J. Eng. Thermophys.*, **22** (2013), 337–345. doi:10.1134/S1810232813040061.
21. K. A. Kumar, J. V. Ramana Reddy, V. Sugunamma and N. Sandeep, MHD Flow of Chemically Reacting Williamson Fluid Over a Curved/Flat Surface with Variable Heat Source/Sink, *Int. J. Fluid Mech. Res.*, **46** (2019), 407-425. doi:10.1615/InterJFluidMechRes.2018025940.
22. K. Ramesh and M. Devakar, Influence of Magnetohydrodynamics on Peristaltic Flow of a Walters B Fluid in an Inclined Asymmetric Channel with Heat Transfer, *World J. Eng.*, **15** (2018), 450-467, doi:10.1108/WJE-09-2017-0305.
23. P. Talebizadehsardari, A. Shahsavar, D. Toghraie and P. Barnoon, An Experimental Investigation for Study the Rheological Behavior of Water–Carbon Nanotube/Magnetite Nanofluid Subjected to a Magnetic Field, *Phys. a Stat. Mech. its Appl.*, **534** (2019), 122129, doi:10.1016/j.physa.2019.122129.
24. H. H. Afrouzi, M. Hosseini, D. Toghraie, E. Mehryaar and M. Afrand, Thermo-Hydraulic Characteristics Investigation of Nanofluid Heat Transfer in a Microchannel with Super Hydrophobic Surfaces Under Non-Uniform Magnetic Field Using Incompressible Preconditioned Lattice Boltzmann Method (IPLBM), *Phys. A Stat. Mech. Its Appl.*, **553** (2020), 124669, doi:10.1016/j.physa.2020.124669.
25. S. A. Shehzad, M. Madhu, N. S. Shashikumar, B. J. Gireesha and B. Mahanthesh, Thermal and Entropy Generation of Non-Newtonian Magneto-Carreau Fluid Flow in Microchannel, *J. Therm. Anal. Calorim.*, (2020), doi:10.1007/s10973-020-09706-8.
26. R. Du, P. Gokulavani, M. Muthtamilselvan, F. Al. Amri and B. Abdalla, Influence of The Lorentz Force on the Ventilation Cavity Having a Centrally Placed Heated Baffle Filled with the Cu-Al₂O₃-H₂O Hybrid Nanofluid, *Int. Commun. Heat Mass Transf.*, **116** (2020), doi:10.1016/j.icheatmasstransfer.2020.104676.
27. M. A. El-Aziz and A. M. Aly, Entropy Generation for Flow and Heat Transfer of Sisko-Fluid Over an Exponentially Stretching Surface, *Comput. Mater. Contin.*, **62** (2020), 37-59, doi:10.32604/cmc.2020.08488.